
FreeSplat: Generalizable 3D Gaussian Splatting Towards Free-View Synthesis of Indoor Scenes

Yunsong Wang Tianxin Huang Hanlin Chen Gim Hee Lee
School of Computing, National University of Singapore
yunsong@comp.nus.edu.sg gimhee.lee@nus.edu.sg
<https://github.com/wangys16/FreeSplat>

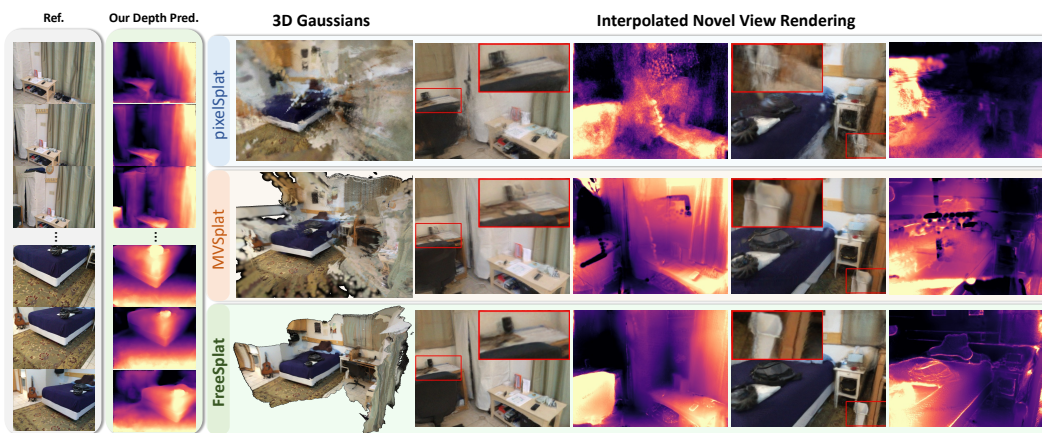


Figure 1: **Comparison between FreeSplat and previous methods.** pixelSplat [1] and MVSplat [2] fail to reconstruct geometrically consistent global 3D Gaussians, while our FreeSplat is proposed to accurately localize 3D Gaussians from long sequence input and support free view synthesis.

Abstract

Empowering 3D Gaussian Splatting with generalization ability is appealing. However, existing generalizable 3D Gaussian Splatting methods are largely confined to narrow-range interpolation between stereo images due to their heavy backbones, thus lacking the ability to accurately localize 3D Gaussian and support free-view synthesis across wide view range. In this paper, we present a novel framework FreeSplat that is capable of reconstructing geometrically consistent 3D scenes from long sequence input towards free-view synthesis. Specifically, we firstly introduce Low-cost Cross-View Aggregation achieved by constructing adaptive cost volumes among nearby views and aggregating features using a multi-scale structure. Subsequently, we present the Pixel-wise Triplet Fusion to eliminate redundancy of 3D Gaussians in overlapping view regions and to aggregate features observed across multiple views. Additionally, we propose a simple but effective free-view training strategy that ensures robust view synthesis across broader view range regardless of the number of views. Our empirical results demonstrate state-of-the-art novel view synthesis performances in both novel view rendered color maps quality and depth maps accuracy across different numbers of input views. We also show that FreeSplat performs inference more efficiently and can effectively reduce redundant Gaussians, offering the possibility of feed-forward large scene reconstruction without depth priors. Our code will be made open-source upon paper acceptance.

1 Introduction

Recent advancements has emerged [3, 4, 5, 6] in reconstructing 3D scenes from multiple viewpoints. Based on ray-marching-based volume rendering, Neural Radiance Fields [3, 7, 8, 9] is capable of learning the implicit 3D geometry and radiance fields without depth information. Nonetheless, computational cost remains to be the inherent bottleneck in ray-marching-based volume rendering, preventing it from real-time rendering. 3D Gaussian Splatting [10, 11, 12, 13] has recently been proposed as an efficient representation for photorealistic reconstruction of 3D scenes from multi-views. The explicit representation of 3D Gaussians are optimized to be densified in the textured regions, and the rasterization-based volume rendering avoids the costly ray marching scheme. Consequently, 3D Gaussian Splatting has achieved real-time rendering of high-quality images from novel views. Nonetheless, vanilla 3D Gaussian Splatting lacks generalizability and requires per-scene optimization.

Several attempts [1, 2, 14, 15, 16, 17] have been made to give 3D Gaussian Splatting generalization ability. Despite showing promising performance, these methods are limited to narrow-range scene-level view interpolation [1, 2, 15] and object-centric synthesis [14, 16]. The primary reason for the limitation is that these existing methods depend on dense view matching across multi-view images with transformers to predict Gaussian primitives, which consequently becomes computationally intractable with longer sequences and thus restricting the supervision of these methods to narrow-range interpolated views. As we show in Figure 3, supervision by narrow-range interpolated views often result in poorly localized 3D Gaussians that can become floaters when rendered from extrapolated views. Additionally, the problem is further aggravated by existing methods typically merging multi-view 3D Gaussians through simple concatenation and thus inevitably lead to noticeable redundancy in overlapping areas (*cf.* Table 2). In view of the above-mentioned problems, it is therefore imperative to design a method that is capable of long sequence reconstruction of global 3D Gaussians, which has the significant potential of supporting real-time rendering from arbitrary poses.

In this paper, we propose FreeSplat tailored for indoor long sequence free view synthesis. Unlike existing methods limited to view interpolation in narrow ranges, our method can effectively reconstruct explicit global 3DGS for novel view synthesis across wide view ranges. Our pipeline consists of Low-cost Cross-View Aggregation and Pixel-wise Triplet Fusion (PTF). In Low-cost Cross-View Aggregation, we introduce efficient CNN-based backbones and adaptive cost volumes formulation among nearby views for low-cost feature extraction and matching, then we leverage a Multi-Scale Feature Aggregation structure to broaden the receptive field of cost volume and predict Depths and Gaussian Triplets. Subsequently, we present Pixel-wise Alignment with progressive Gaussian fusion in PTF to adaptively fuse local Gaussian Triplets from multi-views and avoid Gaussian redundancy in the overlapping regions. Moreover, due to our efficient feature extraction and matching, we propose a Free-View Training (FVT) strategy to disentangle generalizable 3DGS with specific number of views and train the model on long sequences.

The **contributions** of our paper are summarized as follows:

1. We present Low-cost Cross-View Aggregation to predict initial Gaussian triplets, where the low computational cost makes it possible for feature matching between more nearby views and training on long sequence reconstruction;
2. We propose Pixel-wise Triplet Fusion to fuse Gaussian triplets, which can effectively reduce the Gaussian redundancy in the overlapping regions and aggregate multi-view 3D Gaussian latent features;
3. To the best of our knowledge, we are the first to explore generalizable 3DGS for long sequence reconstruction. Extensive experiments on indoor dataset ScanNet [18] and Replica [19] demonstrate our superiority on both image rendering quality and novel view depth rendering accuracy when given different lengths of input views.

2 Related Work

Novel View Synthesis. Traditional attempts in novel view synthesis mainly employed voxel grids [20, 21] or multiplane images [22]. Recently, Neural Radiance Fields (NeRF) [3, 5, 23, 24, 25] have drawn growing interest using ray-marching-based volume rendering to backpropagate image color error to the implicit geometry and radiance fields, such that the 3D geometry can be implicitly learned

to satisfy the multi-view color consistency. Nonetheless, one inherent bottleneck of NeRF-based method is the computation intensity of ray marching, which requires the costly volume sampling in the implicit fields for each pixel during rendering. To this end, recently 3DGS [10, 26, 27, 11] have attracted increasing attention due to its high efficiency and photorealistic rendering. Instead of relying on MLPs to represent the coordinate-based implicit fields, 3DGS learns an explicit field using a set of 3D Gaussians. They optimize the 3D Gaussians parameters and perform adaptive density control to fit to the given set of images, such that the 3D Gaussians are encouraged to perform densification only in the textured regions and refrain from over-densification. During rendering, 3DGS performs tile-based rasterization to differentially accumulate color images from the explicit 3D Gaussian primitives, which is significantly faster than the ray-marching-based volume rendering and achieves real-time rendering speed.

Generalizable Novel View Synthesis. Another drawback of the traditional NeRF-based and 3DGS-based methods is the requirement of per-scene optimization instead of direct feeding-forward. To this end, there have been a line of work [28, 8, 7, 29] focusing on learning effective priors to predict 3D geometry from given images in a feed forward fashion, where the common practice is to project ray-marching sampled points onto given source views to aggregate multi-view features, conditioning the prediction of the implicit fields on source views instead of point coordinates. Recently, there have also been attempts towards generalizable 3DGS [1, 17, 2, 15, 14]. pixelSplat [1] and GPS-Gaussian [17] propose to predict pixel-aligned 3D Gaussian parameters in feed forward fashion. MVSPat [2] replaces the epipolar line transformer of pixelSplat with a lightweight cost volume to perform more efficient image encoding. GGRt [15] concatenates pixelSplat predicted 3D Gaussians in a sequence of images and simultaneously perform pose optimization. latentSplat [14] encodes 3D Variational Gaussians and leverages a discriminator to help produce more indistinguishable images. Nonetheless, existing methods do not reconstruct the global 3D Gaussians from arbitrary length of inputs, and are limited to view interpolation [1, 2, 17, 15] or object/human-centric scenes [17, 14]. In contrary, in this paper we focus on reconstructing large scenes from arbitrary length of inputs without depth priors, unleashing the potential of generalizable 3DGS for large scene explicit representation.

Indoor Scene Reconstruction. One line of efforts in feed-forward indoor scene reconstruction focuses on extracting 3D mesh using voxel volumes [30, 31, 32] and TSDF-fusion [33], while do not perform photorealistic novel view synthesis. On the other hand, the SLAM-based methods [34, 35, 36] require dense sequence of RGB-D input and per-scene tracking and mapping. Another paradigm of 3D reconstruction [37, 38, 39] learns implicit Signed Distance Fields from RGB input, while demanding intensive per-scene optimization. Another recent work SurfelNeRF [40] learns a feed-forward framework to map a sequence of images to 3D surfels which support photorealistic image rendering, while they rely on external depth estimator or ground truth depth maps. In contrary, we propose an end-to-end model without ground truth depth map input or supervision, enabling accurate 3D Gaussian localization using only photometric losses.

3 Preliminary

Vanilla 3DGS. 3D-GS [10] explicitly represents a 3D scene with a set of Gaussian primitives which are parameterized via a 3D covariance matrix Σ and mean μ :

$$G(\mathbf{p}) = \exp\left(-\frac{1}{2}(\mathbf{p} - \mu)^\top \Sigma^{-1}(\mathbf{p} - \mu)\right), \quad (1)$$

where Σ is decomposed into $\Sigma = \mathbf{R}\mathbf{S}\mathbf{S}^\top\mathbf{R}^\top$ using a scaling matrix \mathbf{S} and a rotation matrix \mathbf{R} to maintain positive semi-definiteness. During rendering, the 3D Gaussian is transformed into the image coordinates with world-to-camera transform matrix \mathbf{W} and projected onto image plane with projection matrix \mathbf{J} , and the 2D covariance matrix Σ' is computed as $\Sigma' = \mathbf{J}\mathbf{W}\Sigma\mathbf{W}^\top\mathbf{J}^\top$. We then obtain a 2D Gaussian G^{2D} with the covariance Σ' in 2D, and the color rendering is computed using point-based alpha-blending on each ray:

$$\mathbf{C}(\mathbf{x}) = \sum_{i \in N} \mathbf{c}_i \alpha_i G_i^{2D}(\mathbf{x}) \prod_{j=1}^{i-1} (1 - \alpha_j G_j^{2D}(\mathbf{x})), \quad (2)$$

where N is the number of Gaussian primitives, α_i is a learnable opacity, and \mathbf{c}_i is view-dependent color defined by spherical harmonics (SH) coefficients \mathbf{s} . The Gaussian parameters are optimized by a photometric loss to minimize the difference between renderings and image observations.

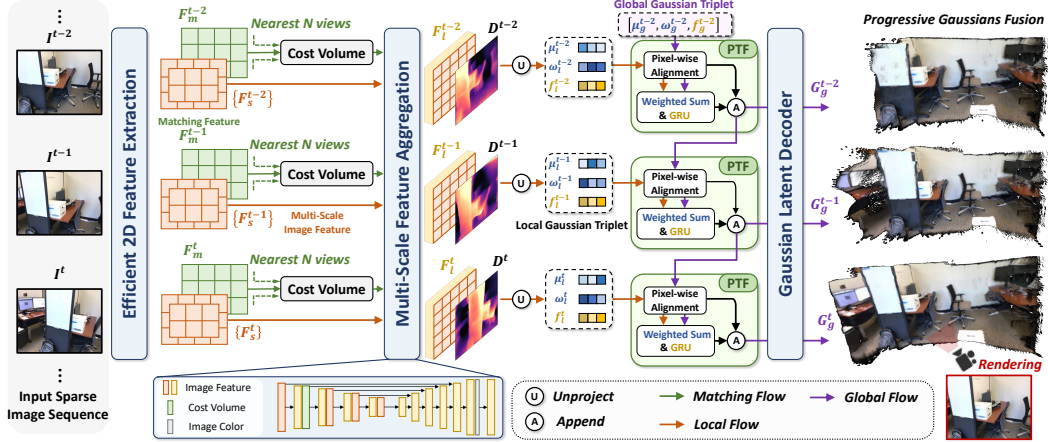


Figure 2: **Framework of FreeSplat.** Given input sparse sequence of images, we construct cost volumes between nearby views and predict depth maps and corresponding feature maps, followed by unprojection to Gaussian triplets with 3D positions. We then propose **Pixel-aligned Triplet Fusion (PTF)** module, where we progressively aggregate and update local/global Gaussian triplets based on pixel-wise alignment. The global Gaussian triplets can be later decoded into Gaussian parameters.

Generalizable 3DGS. Unlike vanilla 3DGS that optimizes per-scene Gaussian primitives, recent generalizable 3DGS [1, 17] predict pixel-aligned Gaussian primitives $\{\Sigma, \alpha, s\}$ and depths d , such that the pixel-aligned Gaussian primitives can be unprojected to 3D coordinates μ . The Gaussian parameters are predicted by 2D encoders, which are optimized by the photometric loss through rendering from novel views. However, existing methods are still limited to view interpolation within narrow view range, which leads to inaccurately localized 3D Gaussians that fail to support large scene reconstruction and view extrapolation (*cf.* Figure 1, 3). To this end, we propose FreeSplat towards global 3D Gaussians reconstruction with accurate localization that supports free-view synthesis.

4 Our Methodology

4.1 Overview

The overview of our method is illustrated in Figure 2. Given a sparse sequence of RGB images, we build cost volumes adaptively between nearby views, and predict depth maps to unproject the 2D feature maps into 3D Gaussian triplets. We then propose the Pixel-aligned Triplet Fusion (PTF) module to progressively align the global with the local Gaussian triplets, such that we can fuse the redundant 3D Gaussians in the latent feature space and aggregate cross-view Gaussian features before decoding. Our method is capable of efficiently exchanging cross-view features through cost volumes, and progressively aggregating per-view 3D Gaussians with cross-view alignment and adaptive fusion.

4.2 Low-cost Cross-View Aggregation

Efficient 2D Feature Extraction. Given a sparse sequence of posed images $\{I^t\}_{t=1}^T$, we first feed them into a shared 2D backbone to extract multi-scale embeddings F_e^t . To decrease and computational cost in plane sweeping, we train a matching net [41] to embed the low-dimensional matching feature F_m^t . Unlike [1, 2] which rely on patch-wise transformer-based backbones [42, 43] that can lead to quadratically expensive computations, we leverage pure CNN-based backbones [44, 41] for 2D feature extraction for efficient performance on higher resolution inputs.

Adaptive Cost Volume Formulation. To explicitly integrate camera pose information given arbitrary length of input images, we propose to adaptively build cost volumes between nearby views. For current view I^t with pose P^t and matching feature $F_m^t \in \mathbb{R}^{C_m \times \frac{H}{4} \times \frac{W}{4}}$, we adaptively select its N nearby views $\{I^{t_n}\}_{n=1}^N$ with poses $\{P^{t_n}\}_{n=1}^N$ based on pose proximity, and construct cost volume via plane sweep stereo [45, 46]. Specifically, we define a set of K virtual depth planes $\{d_k\}_{k=1}^K$ that are uniformly spaced within $[d_{near}, d_{far}]$, and warp the nearby view features to each depth plane d_k

of current view:

$$\tilde{\mathbf{F}}_m^{t_n,k} = \text{Trans}(\mathbf{P}^{t_n}, \mathbf{P}^t) \mathbf{F}_m^{t_n}, \quad (3)$$

where $\text{Trans}(\mathbf{P}^{t_n}, \mathbf{P}^t)$ is the transformation matrix from view t_n to t . The cost volume $\mathbf{F}_{\text{cv}}^t \in \mathbb{R}^{K \times \frac{H}{4} \times \frac{W}{4}}$ is then defined as:

$$\mathbf{F}_{\text{cv}}^t(k) = f_\theta \left(\left(\frac{1}{N} \sum_{n=1}^N \cos(\mathbf{F}_m^t, \tilde{\mathbf{F}}_m^{t_n,k}) \right) \oplus \left(\frac{1}{N} \sum_{n=1}^N \tilde{\mathbf{F}}_m^{t_n,k} \right) \right), \quad (4)$$

where $\mathbf{F}_{\text{cv}}^t[k]$ is the k -th dimension of \mathbf{F}_{cv}^t , $\cos(\cdot)$ is the cosine similarity, \oplus is feature-wise concatenation, and $f_\theta(\cdot)$ is a 1×1 CNN mapping to dimension of 1.

Multi-Scale Feature Aggregation. The embedding of the cost volume plays a significant part to accurately localize the 3D Gaussians (*cf.* Table 5, 6). To this end, inspired by previous depth estimation methods [47, 33], we design an multi-scale encoder-decoder structure, such that to fuse multi-scale image features with the cost volume and propagate the cost volume information to broader receptive fields. Specifically, the multi-scale encoder takes in \mathbf{F}_{cv}^t and the output is concatenated with $\{\mathbf{F}_s^t\}$ before sending into a UNet++ [48]-like decoder to upsample to full resolution and predict a depth candidates map $\mathbf{D}_c^t \in \mathbb{R}^{K \times H \times W}$, and Gaussian triplet map $\mathbf{F}_l^t \in \mathbb{R}^{C \times H \times W}$. We then predict the depth map through soft-argmax to bound the depth prediction between near and far:

$$\mathbf{D}^t = \sum_{k=1}^K \text{softmax}(\mathbf{D}_c^t)_k \cdot d_k. \quad (5)$$

Finally, the pixel-aligned Gaussian triplet map \mathbf{F}_l^t is unprojected to 3D Gaussian triplet $\{\boldsymbol{\mu}_l^t, \boldsymbol{\omega}_l^t, \mathbf{f}_l^t\}$, where $\boldsymbol{\mu}_l^t \in \mathbb{R}^{3 \times HW}$ are the Gaussian centers, $\boldsymbol{\omega}_l^t \in \mathbb{R}^{1 \times HW}$ are weights between (0, 1), and $\mathbf{f}_l^t \in \mathbb{R}^{(C-1) \times HW}$ are Gaussian triplet features.

4.3 Pixel-wise Triplet Fusion

One limitation of previous generalizable 3DGS methods is the redundancy of Gaussians. Since we need multi-view observations to predict accurately localized 3D Gaussians in indoor scenes, the pixel-aligned Gaussians become redundant in frequently observed regions. Furthermore, previous methods integrate multi-view Gaussians of the same region simply through their opacities, leading to suboptimal performance due to lack of post aggregation (*cf.* Table 5). Consequently, inspired by previous methods [31, 40], we propose the Pixel-wise Triplet Fusion (PTF) module which can significantly remove redundant Gaussians in the overlapping regions and explicitly aggregate multi-view observation features in the latent space. We align the per-view local Gaussians with global ones using Pixel-wise Alignment to select the redundant 3D Gaussian Triplets, and progressively fuse the local Gaussians into the global ones.

Pixel-wise Alignment. Given the Gaussian triplets $\{\boldsymbol{\mu}_l^t, \mathbf{f}_l^t\}_{t=1}^T$, we start from $t = 1$ where the global Gaussians latent is empty. In t -th step, we first project the global Gaussian triplet centers $\boldsymbol{\mu}_g^{t-1} \in \mathbb{R}^{3 \times M}$ onto the t -th view:

$$\mathbf{p}_g^t := \{\mathbf{x}_g^t, \mathbf{y}_g^t, \mathbf{d}_g^t\} = \mathbf{P}^t \boldsymbol{\mu}_g^{t-1}, \quad (6)$$

where $[\mathbf{x}_g^t, \mathbf{y}_g^t, \mathbf{d}_g^t] \in \mathbb{R}^{3 \times M}$ are the projected 2D coordinates and corresponding depths. We then correspond the local Gaussian triplets with the pixel-wise nearest projections within a threshold. Specifically, for the i -th local Gaussian with 2D coordinate $[\mathbf{x}_l^t(i), \mathbf{y}_l^t(i)]$ and depth $\mathbf{d}_l^t(i)$, we first find its intra-pixel global projection set \mathcal{S}_i :

$$\mathcal{S}_i^t := \{j \mid [\mathbf{x}_g^t(j)] = \mathbf{x}_l^t(i), [\mathbf{y}_g^t(j)] = \mathbf{y}_l^t(i)\}, \quad (7)$$

where $[\cdot]$ is rounding. Subsequently, we search for valid correspondence with minimum depth difference under a threshold:

$$m_i = \begin{cases} \arg \min_{j \in \mathcal{S}_i^t} \mathbf{d}_g^t(j) & \text{if } |\mathbf{d}_l^t(i) - \min_{j \in \mathcal{S}_i^t} \mathbf{d}_g^t(j)| < \delta \cdot \mathbf{d}_l^t(i) \\ \emptyset & \text{otherwise} \end{cases}, \quad (8)$$

where δ is a ratio threshold. We define the valid correspondence set as:

$$\mathcal{F}^t := \{(i, m_i) \mid i = 1, \dots, HW; m_i \neq \emptyset\}. \quad (9)$$

Gaussian Triplet Fusion. After the pixel-wise alignment, we remove the redundant 3D Gaussians through merging the validly aligned triplet pairs. Given a pair $(i, m_i) \in \mathcal{F}^t$, to restrict the 3D Gaussian centers to lie between the triplet pair, we weighted sum their center coordinates and sum their weights:

$$\boldsymbol{\mu}_g^t(m_i) = \frac{\boldsymbol{\omega}_l^t(i)\boldsymbol{\mu}_l^t(i) + \boldsymbol{\omega}_g^{t-1}(m_i)\boldsymbol{\mu}_g^{t-1}(m_i)}{\boldsymbol{\omega}_l^t(i) + \boldsymbol{\omega}_g^t(m_i)}, \quad (10)$$

$$\boldsymbol{\omega}_g^t(m_i) = \boldsymbol{\omega}_l^t(i) + \boldsymbol{\omega}_g^{t-1}(m_i). \quad (11)$$

To aggregate the local and global Gaussian latent features, we update the global Gaussian latent feature through a lightweight GRU network:

$$\mathbf{f}_g^t(m_i) = \text{GRU}(\mathbf{f}_l^t(i), \mathbf{f}_g^{t-1}(m_i)) \quad (12)$$

Then the other local Gaussian triplets are appended to the global ones.

Gaussian primitives decoding. After the Pixel-wise Triplet Fusion, we can decode the global Gaussian triplets into Gaussian primitives:

$$\boldsymbol{\Sigma}, \boldsymbol{\alpha}, \mathbf{s} = \text{MLP}_d(\mathbf{f}_g^T) \quad (13)$$

and the Gaussian centers $\boldsymbol{\mu} = \boldsymbol{\mu}_g^T$. Our proposed fusion method can incrementally integrate the Gaussians with geometrical constraints and learnable GRU network for feature update, which is capable of significantly removing redundant Gaussians and perform post feature aggregation across multiple views, and can be trained with the other framework components end-to-end with eligible computation overhead.

4.4 Training

Loss Functions. After predicting the 3D Gaussian primitives, we render from novel views following the rendering equations in Eq. (2). Similar to pixelSplat [1] and MVSpLat [2], we train our framework using only photometric losses, *i.e.* a combination of MSE loss and LPIPS [49] loss, with weights of 1 and 0.05 following [1, 2].

Free-View Training. We propose a Free-View Training (FVT) strategy to add more geometrical constraints on the localization of 3D Gaussians, and to disentangle the performance of generalizable 3DGS with specific number of input views. To this end, we randomly sample T number of context views (in experiments we set T between 2 and 8), and supervise the image renderings in the broader view interpolations. The long sequence training is made feasible due to our efficient feature extraction and aggregation. We empirically find that FVT significantly contributes to depth estimation from novel views (*cf.* Table 3, 4).

5 Experiments

5.1 Experimental Settings

Datasets. We leverage the real-world indoor dataset ScanNet [18] for training. ScanNet is a large RGB-D dataset containing 1,513 indoor scenes with camera poses, and we follow [50, 40] to use 100 scenes for training and 8 scenes for testing. To evaluate the generalization ability of our model, we further perform zero-shot evaluation on the synthetic indoor dataset Replica [19], for which we follow [51] to select 8 scenes for testing.

Implementation Details. Our FreeSplat is trained end-to-end using Adam [52] optimizer with an initial learning rate of $1e-4$ for 300k iterations following [1, 2]. Due to the large GPU requirements of [1, 2] given high-resolution images, all input images are resized to 512×384 and batch size is set to 1, to form a fair comparison between different methods. We mainly compare with previous generalizable 3DGS methods in 2, 3, 10 reference view settings to evaluate the models’ performance under different length of input views. For 10 views setting, we also choose target views that are beyond the given sequence of reference views to evaluate the view extrapolation results. Furthermore, we notice that in MVSpLat there is a misalignment between the depth plane candidates and the unprojection (more discussion in Appendix A.3), which we modified and report their improved version in the following unless otherwise specified.

Table 1: **Generalizable Novel View Interpolation results on ScanNet [18]**. Except for FreeSplat-*fv*, other methods are all trained on specific number of views to form a complete comparison. Time(s) indicates the total time of encoding input images and rendering one image.

Method	2 views					3 views				
	PSNR \uparrow	SSIM \uparrow	LPIPS \downarrow	Time(s) \downarrow	#GS(k)	PSNR \uparrow	SSIM \uparrow	LPIPS \downarrow	Time(s) \downarrow	#GS(k)
NeuRay [9]	25.65	0.840	0.264	3.103	-	25.47	0.843	0.264	4.278	-
pixelSplat [1]	26.03	0.784	0.265	0.289	1180	25.76	0.782	0.270	0.272	1769
MVSplat [2]	25.05	0.771	0.258	0.105	393	24.24	0.769	0.273	0.192	590
FreeSplat-spec	27.70	0.826	0.222	0.095	292	27.24	0.820	0.232	0.101	384
FreeSplat-fv	27.18	0.818	0.226	0.097	296	26.79	0.813	0.238	0.104	393

Table 2: **Long Sequence (10 views) Explicit Reconstruction results on ScanNet**. The results of pixelSplat, MVSplat and FreeSplat-*spec* are given using their 3-views version.

Method	Time(s) \downarrow	#GS(k)	View Interpolation			View Extrapolation		
			PSNR \uparrow	SSIM \uparrow	LPIPS \downarrow	PSNR \uparrow	SSIM \uparrow	LPIPS \downarrow
pixelSplat [1]	0.948	5898	21.26	0.714	0.396	20.70	0.687	0.429
MVSplat [2]	1.178	1966	18.87	0.664	0.417	18.72	0.642	0.444
FreeSplat-spec	0.273	1071	23.06	0.755	0.354	22.30	0.722	0.391
FreeSplat-fv	0.307	958	24.91	0.792	0.278	24.05	0.773	0.304

5.2 Results on ScanNet

View Interpolation Results. On ScanNet, we evaluate the generalizable novel view interpolation results given 2 and 3 reference views as shown in Table 1. Comparing to pixelSplat and MVSplat, our FreeSplat-*spec* consistently improves PSNR by over 1.67 dB on 2-views setting and 1.48 dB on 3-views setting. Although slightly underperforming on SSIM comparing to NeuRay [9], we show significant improvements on PSNR and LPIPS over NeuRay and $300\times$ faster inference speed. Moreover, our FreeSplat-*fv* consistently offers competitive results given arbitrary number of views.

Long Sequence Results. We further evaluate the long sequence results where we sample reference views with length of 10, and compare both view interpolation and extrapolation results as shown in Table 2. The results reveal that generalizable 3DGS methods underperform when given long sequence input images, which is due to the complicated camera trajectories in ScanNet, and the inaccuracy of 3D Gaussian localization that leads to errors when observed beyond the interpolated views. Our FreeSplat-*3views* still outperforms pixelSplat and MVSplat by over 1.80 dB PSNR on view interpolation and 1.60 dB PSNR on view extrapolation results. Through our proposed FVT that can be easily plugged into our model due to our low requirement on GPU, our FreeSplat-*fv* significantly outperforms our 3-views version by over 1.85 dB PSNR. Our PTF module can also reduce the number of Gaussians by 45.5% – 51.3%, which significantly contributes to the efficiency of 3D Gaussians when given long sequence inputs. The qualitative results are shown in Figure 3, where the results clearly reveal that FreeSplat-*spec* outperforms MVSplat and pixelSplat in localizing 3D Gaussian and preserving fine-grained details, and FreeSplat-*fv* further improves on localizing and fusing multi-view Gaussians.

Table 3: **Novel View Depth Rendering results on ScanNet**. \dagger : 10-views results of pixelSplat, MVSplat and FreeSplat-*spec* are given using their 3-views version.

Method	2 views				3 views			10 views \dagger		
	Abs Diff \downarrow	Abs Rel \downarrow	$\delta < 1.25 \uparrow$	Abs Diff \downarrow	Abs Rel \downarrow	$\delta < 1.25 \uparrow$	Abs Diff \downarrow	Abs Rel \downarrow	$\delta < 1.25 \uparrow$	
NeuRay [9]	0.358	0.200	0.755	0.231	0.117	0.873	0.202	0.108	0.875	
pixelSplat [1]	1.205	0.745	0.472	0.698	0.479	0.836	0.970	0.621	0.647	
MVSplat [2]	0.526	0.274	0.396	0.394	0.201	0.625	0.423	0.240	0.558	
FreeSplat-spec	0.239	0.121	0.833	0.218	0.108	0.882	0.214	0.122	0.850	
FreeSplat-fv	0.220	0.117	0.847	0.209	0.099	0.888	0.159	0.092	0.917	

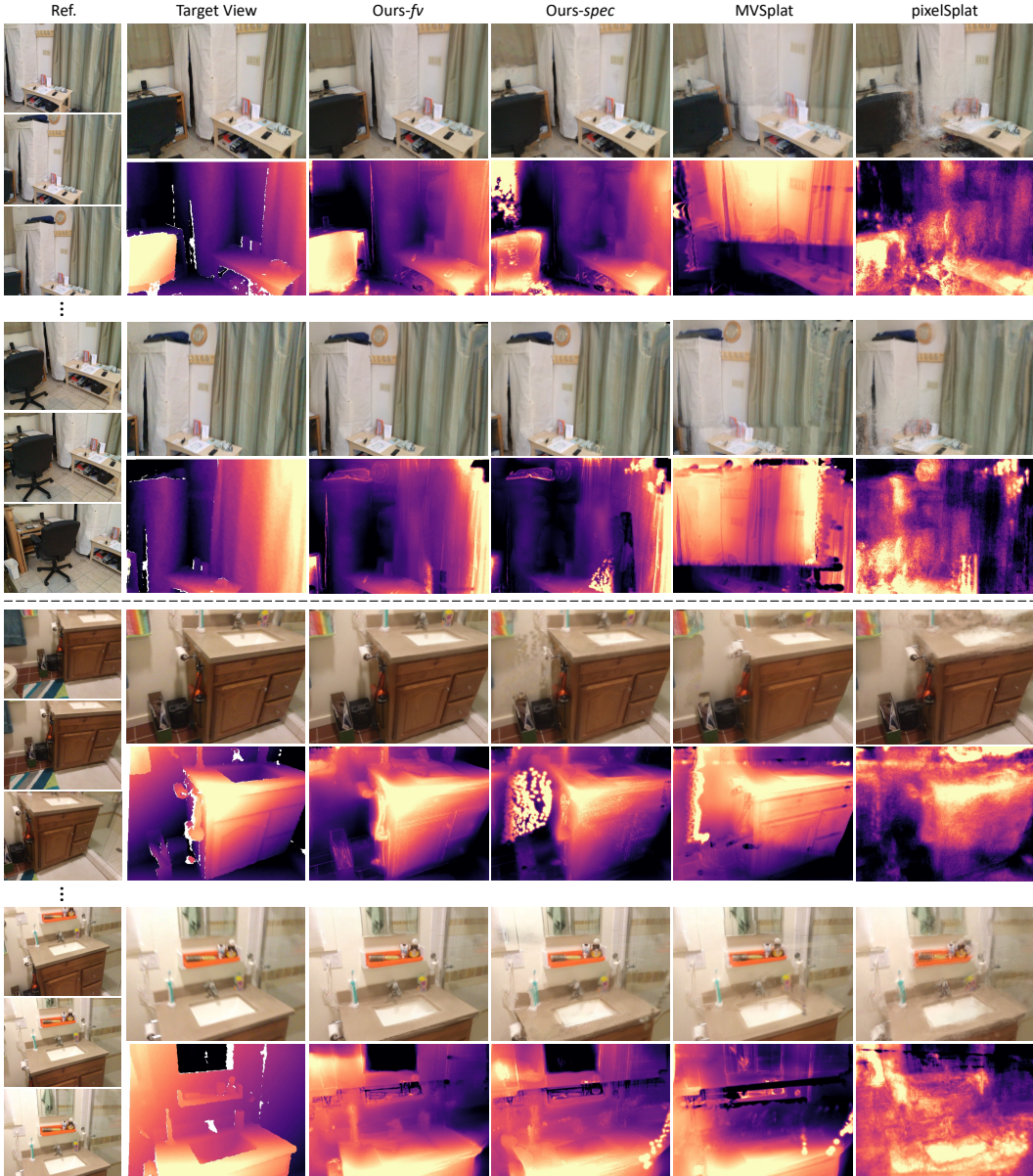


Figure 3: **Qualitative Results of Long Sequence Explicit Reconstruction.** For each sequence, the first two rows are view interpolation results, and the last two rows are view extrapolation results.

Novel View Depth Estimation Results. We also investigate the correctness of 3D Gaussian localization of different methods through comparing their depth rendering results. We report the Absolute Difference (Abs. Diff), Relative Difference (Rel. Diff), and threshold tolerance $\delta < 1.25$ results from novel views in Table 3. We find that FreeSplat significantly outperforms pixelSplat and MVSplat in predicting accurately localized 3D Gaussians, where FreeSplat-*fv* reaches 91.7% of $\delta < 1.25$, outperforming pixelSplat and MVSplat by over 27.0%, enabling accurate unsupervised depth estimation from novel views. The improved depth estimation accuracy of FreeSplat-*fv* highlights the importance of depth estimation in supporting free-view synthesis across broader view range.

5.3 Zero-Shot Transfer Results on Replica

We further evaluate the zero-shot transfer results through testing on Replica dataset, with results in Table 4. Our view interpolation and novel view depth estimation results still outperforms existing

Table 4: **Zero-Shot Transfer Results on Replica [19].**

Method	3 Views					10 Views				
	PSNR \uparrow	SSIM \uparrow	LPIPS \downarrow	$\delta < 1.25 \uparrow$	#GS(k)	PSNR \uparrow	SSIM \uparrow	LPIPS \downarrow	$\delta < 1.25 \uparrow$	#GS(k)
pixelSplat [1]	26.24	0.829	0.229	0.576	1769	19.23	0.719	0.414	0.375	5898
MVSplat [2]	21.51	0.749	0.267	0.295	590	16.06	0.644	0.459	0.203	1966
FreeSplat-spec	27.08	0.848	0.175	0.657	415	19.83	0.735	0.361	0.585	1571
FreeSplat-fv	26.28	0.834	0.193	0.655	429	20.99	0.757	0.322	0.665	1478

Table 5: **Ablation on ScanNet.** CV: Cost Volume, PTF: Pixel-wise Triplet Fusion, FVT: Free-View Training.

CV	PTF	FVT	3 views					10 views				
			PSNR \uparrow	SSIM \uparrow	LPIPS \downarrow	Abs Diff \downarrow	$\delta < 1.25 \uparrow$	PSNR \uparrow	SSIM \uparrow	LPIPS \downarrow	Abs Diff \downarrow	$\delta < 1.25 \uparrow$
✓			26.92	0.810	0.241	0.233	0.869	22.58	0.739	0.363	0.231	0.836
	✓		22.10	0.696	0.359	0.393	0.639	17.94	0.607	0.487	0.447	0.543
		✓	27.24	0.820	0.232	0.218	0.882	23.06	0.755	0.354	0.214	0.850
✓	✓		25.94	0.790	0.254	0.237	0.860	24.22	0.760	0.310	0.169	0.899
✓	✓	✓	26.79	0.813	0.238	0.209	0.879	24.91	0.792	0.278	0.159	0.917

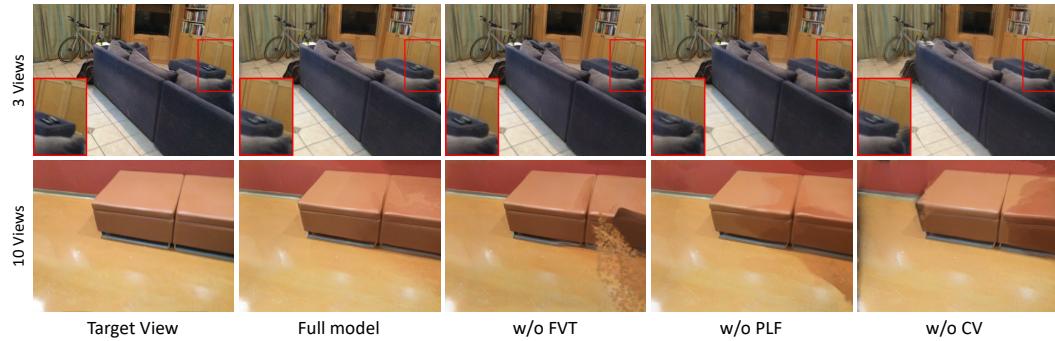


Figure 4: **Qualitative Ablation Study.** The first and second row use input view lengths of 3 and 10.

methods. The long sequence results degrade due to inaccurate depth estimation and domain gap, indicating potential future work in further improving the depth estimation in zero-shot transferring.

5.4 Ablation Study

We conduct a detailed ablation study as shown in Table 5 and Figure 4. The results indicate that cost volume is essential in accurately localizing 3D Gaussians, and our proposed PTF module can consistently contribute to rendering quality and depth estimation results through its post aggregation of Gaussians. Furthermore, our FVT module excels in long sequence reconstruction results as well as novel view depth rendering results, indicating its significance in the unsupervised learning of depth estimation and reconstructing geometrically sound scenes.

6 Conclusion

In this study, we introduced FreeSplat, a generalizable 3DGS model that is tailored to accommodate an arbitrary number of input views and perform free-view synthesis using the global 3D Gaussians. We developed a Low-cost Cross-View Aggregation pipeline that enhances the model’s ability to efficiently process long input sequences, thus incorporating stricter geometry constraints. Additionally, we have devised a Pixel-wise Triplet Fusion module that effectively reduces redundant pixel-aligned 3D Gaussians in overlapping regions and merges multi-view Gaussian latent features. FreeSplat consistently improves the fidelity of novel view renderings in terms of both color image quality and depth map accuracy, facilitating feed-forward global Gaussians reconstruction without depth priors.

References

- [1] David Charatan, Sizhe Li, Andrea Tagliasacchi, and Vincent Sitzmann. pixelsplat: 3d gaussian splats from image pairs for scalable generalizable 3d reconstruction. *arXiv preprint arXiv:2312.12337*, 2023.
- [2] Yuedong Chen, Haofei Xu, Chuanxia Zheng, Bohan Zhuang, Marc Pollefeys, Andreas Geiger, Tat-Jen Cham, and Jianfei Cai. Mvsplat: Efficient 3d gaussian splatting from sparse multi-view images. *arXiv preprint arXiv:2403.14627*, 2024.
- [3] Ben Mildenhall, Pratul Srinivasan, Matthew Tancik, Jonathan Barron, Ravi Ramamoorthi, and Ren Ng. Nerf: Representing scenes as neural radiance fields for view synthesis. In *European Conference on Computer Vision*, pages 405–421. Springer, 2020.
- [4] Peng Wang, Lingjie Liu, Yuan Liu, Christian Theobalt, Taku Komura, and Wenping Wang. Neus: Learning neural implicit surfaces by volume rendering for multi-view reconstruction. *arXiv preprint arXiv:2106.10689*, 2021.
- [5] Thomas Müller, Alex Evans, Christoph Schied, and Alexander Keller. Instant neural graphics primitives with a multiresolution hash encoding. *ACM Transactions on Graphics (ToG)*, 41(4):1–15, 2022.
- [6] Jonathan T Barron, Ben Mildenhall, Dor Verbin, Pratul P Srinivasan, and Peter Hedman. Mipnerf 360: Unbounded anti-aliased neural radiance fields. In *Proceedings of the IEEE/CVF Conference on Computer Vision and Pattern Recognition*, pages 5470–5479, 2022.
- [7] Qianqian Wang, Zhicheng Wang, Kyle Genova, Pratul Srinivasan, Howard Zhou, Jonathan T. Barron, Ricardo Martin-Brualla, Noah Snavely, and Thomas Funkhouser. Ibrnet: Learning multi-view image-based rendering. In *CVPR*, 2021.
- [8] Anpei Chen, Zexiang Xu, Fuqiang Zhao, Xiaoshuai Zhang, Fanbo Xiang, Jingyi Yu, and Hao Su. Mvsnerf: Fast generalizable radiance field reconstruction from multi-view stereo. In *Proceedings of the IEEE/CVF International Conference on Computer Vision*, pages 14124–14133, 2021.
- [9] Yuan Liu, Sida Peng, Lingjie Liu, Qianqian Wang, Peng Wang, Christian Theobalt, Xiaowei Zhou, and Wenping Wang. Neural rays for occlusion-aware image-based rendering. In *Proceedings of the IEEE/CVF Conference on Computer Vision and Pattern Recognition*, pages 7824–7833, 2022.
- [10] Bernhard Kerbl, Georgios Kopanas, Thomas Leimkühler, and George Drettakis. 3d gaussian splatting for real-time radiance field rendering. *ACM Transactions on Graphics*, 42(4):1–14, 2023.
- [11] Zehao Yu, Anpei Chen, Binbin Huang, Torsten Sattler, and Andreas Geiger. Mip-splatting: Alias-free 3d gaussian splatting. *arXiv preprint arXiv:2311.16493*, 2023.
- [12] Kerui Ren, Lihan Jiang, Tao Lu, Mulin Yu, Linning Xu, Zhangkai Ni, and Bo Dai. Octreegs: Towards consistent real-time rendering with lod-structured 3d gaussians. *arXiv preprint arXiv:2403.17898*, 2024.
- [13] Jonathon Luiten, Georgios Kopanas, Bastian Leibe, and Deva Ramanan. Dynamic 3d gaussians: Tracking by persistent dynamic view synthesis. *arXiv preprint arXiv:2308.09713*, 2023.
- [14] Christopher Wewer, Kevin Raj, Eddy Ilg, Bernt Schiele, and Jan Eric Lenssen. latentsplat: Autoencoding variational gaussians for fast generalizable 3d reconstruction. *arXiv preprint arXiv:2403.16292*, 2024.
- [15] Hao Li, Yuanyuan Gao, Dingwen Zhang, Chenming Wu, Yalun Dai, Chen Zhao, Haocheng Feng, Errui Ding, Jingdong Wang, and Junwei Han. Ggrt: Towards generalizable 3d gaussians without pose priors in real-time. *arXiv preprint arXiv:2403.10147*, 2024.
- [16] Zi-Xin Zou, Zhipeng Yu, Yuan-Chen Guo, Yangguang Li, Ding Liang, Yan-Pei Cao, and Song-Hai Zhang. Triplane meets gaussian splatting: Fast and generalizable single-view 3d reconstruction with transformers. *arXiv preprint arXiv:2312.09147*, 2023.
- [17] Shunyuan Zheng, Boyao Zhou, Ruizhi Shao, Boning Liu, Shengping Zhang, Liqiang Nie, and Yebin Liu. Gps-gaussian: Generalizable pixel-wise 3d gaussian splatting for real-time human novel view synthesis. *arXiv preprint arXiv:2312.02155*, 2023.

- [18] Angela Dai, Angel X Chang, Manolis Savva, Maciej Halber, Thomas Funkhouser, and Matthias Nießner. Scannet: Richly-annotated 3d reconstructions of indoor scenes. In *Proceedings of the IEEE conference on computer vision and pattern recognition*, pages 5828–5839, 2017.
- [19] Julian Straub, Thomas Whelan, Lingni Ma, Yufan Chen, Erik Wijmans, Simon Green, Jakob J Engel, Raul Mur-Artal, Carl Ren, Shobhit Verma, et al. The replica dataset: A digital replica of indoor spaces. *arXiv preprint arXiv:1906.05797*, 2019.
- [20] Stephen Lombardi, Tomas Simon, Jason Saragih, Gabriel Schwartz, Andreas Lehrmann, and Yaser Sheikh. Neural volumes: Learning dynamic renderable volumes from images. *arXiv preprint arXiv:1906.07751*, 2019.
- [21] Vincent Sitzmann, Justus Thies, Felix Heide, Matthias Nießner, Gordon Wetzstein, and Michael Zollhofer. Deepvoxels: Learning persistent 3d feature embeddings. In *Proceedings of the IEEE/CVF Conference on Computer Vision and Pattern Recognition*, pages 2437–2446, 2019.
- [22] Tinghui Zhou, Richard Tucker, John Flynn, Graham Fyffe, and Noah Snavely. Stereo magnification: Learning view synthesis using multiplane images. *arXiv preprint arXiv:1805.09817*, 2018.
- [23] Jonathan T Barron, Ben Mildenhall, Matthew Tancik, Peter Hedman, Ricardo Martin-Brualla, and Pratul P Srinivasan. Mip-nerf: A multiscale representation for anti-aliasing neural radiance fields. In *Proceedings of the IEEE/CVF International Conference on Computer Vision*, pages 5855–5864, 2021.
- [24] Jonathan T Barron, Ben Mildenhall, Dor Verbin, Pratul P Srinivasan, and Peter Hedman. Mip-nerf 360: Unbounded anti-aliased neural radiance fields. In *Proceedings of the IEEE/CVF Conference on Computer Vision and Pattern Recognition*, pages 5470–5479, 2022.
- [25] Jonathan T Barron, Ben Mildenhall, Dor Verbin, Pratul P Srinivasan, and Peter Hedman. Zip-nerf: Anti-aliased grid-based neural radiance fields. In *Proceedings of the IEEE/CVF International Conference on Computer Vision*, pages 19697–19705, 2023.
- [26] Jonathon Luiten, Georgios Kopanas, Bastian Leibe, and Deva Ramanan. Dynamic 3d gaussians: Tracking by persistent dynamic view synthesis. *arXiv preprint arXiv:2308.09713*, 2023.
- [27] Guanjun Wu, Taoran Yi, Jiemin Fang, Lingxi Xie, Xiaopeng Zhang, Wei Wei, Wenyu Liu, Qi Tian, and Xinggang Wang. 4d gaussian splatting for real-time dynamic scene rendering. *arXiv preprint arXiv:2310.08528*, 2023.
- [28] Alex Yu, Vickie Ye, Matthew Tancik, and Angjoo Kanazawa. pixelnerf: Neural radiance fields from one or few images. In *Proceedings of the IEEE/CVF Conference on Computer Vision and Pattern Recognition*, pages 4578–4587, 2021.
- [29] Michael Niemeyer, Jonathan T Barron, Ben Mildenhall, Mehdi SM Sajjadi, Andreas Geiger, and Noha Radwan. Regnerf: Regularizing neural radiance fields for view synthesis from sparse inputs. In *Proceedings of the IEEE/CVF Conference on Computer Vision and Pattern Recognition*, pages 5480–5490, 2022.
- [30] Songyou Peng, Michael Niemeyer, Lars Mescheder, Marc Pollefeys, and Andreas Geiger. Convolutional occupancy networks. In *Computer Vision—ECCV 2020: 16th European Conference, Glasgow, UK, August 23–28, 2020, Proceedings, Part III 16*, pages 523–540. Springer, 2020.
- [31] Jiaming Sun, Yiming Xie, Linghao Chen, Xiaowei Zhou, and Hujun Bao. Neuralrecon: Real-time coherent 3d reconstruction from monocular video. In *Proceedings of the IEEE/CVF conference on computer vision and pattern recognition*, pages 15598–15607, 2021.
- [32] Noah Stier, Alexander Rich, Pradeep Sen, and Tobias Höllerer. Vortex: Volumetric 3d reconstruction with transformers for voxelwise view selection and fusion. In *2021 International Conference on 3D Vision (3DV)*, pages 320–330. IEEE, 2021.
- [33] Mohamed Sayed, John Gibson, Jamie Watson, Victor Prisacariu, Michael Firman, and Clément Godard. Simplexrecon: 3d reconstruction without 3d convolutions. In *European Conference on Computer Vision*, pages 1–19. Springer, 2022.
- [34] Zihan Zhu, Songyou Peng, Viktor Larsson, Weiwei Xu, Hujun Bao, Zhaopeng Cui, Martin R Oswald, and Marc Pollefeys. Nice-slam: Neural implicit scalable encoding for slam. In *Proceedings of the IEEE/CVF Conference on Computer Vision and Pattern Recognition*, pages 12786–12796, 2022.

- [35] Chi Yan, Delin Qu, Dong Wang, Dan Xu, Zhigang Wang, Bin Zhao, and Xuelong Li. Gs-slam: Dense visual slam with 3d gaussian splatting. *arXiv preprint arXiv:2311.11700*, 2023.
- [36] Nikhil Keetha, Jay Karhade, Krishna Murthy Jatavallabhula, Gengshan Yang, Sebastian Scherer, Deva Ramanan, and Jonathon Luiten. Splatam: Splat, track & map 3d gaussians for dense rgb-d slam. *arXiv preprint arXiv:2312.02126*, 2023.
- [37] Lior Yariv, Jiatao Gu, Yoni Kasten, and Yaron Lipman. Volume rendering of neural implicit surfaces. *Advances in Neural Information Processing Systems*, 34:4805–4815, 2021.
- [38] Zehao Yu, Songyou Peng, Michael Niemeyer, Torsten Sattler, and Andreas Geiger. Monosdf: Exploring monocular geometric cues for neural implicit surface reconstruction. *Advances in neural information processing systems*, 35:25018–25032, 2022.
- [39] Zhaoshuo Li, Thomas Müller, Alex Evans, Russell H Taylor, Mathias Unberath, Ming-Yu Liu, and Chen-Hsuan Lin. Neuralangelo: High-fidelity neural surface reconstruction. In *Proceedings of the IEEE/CVF Conference on Computer Vision and Pattern Recognition*, pages 8456–8465, 2023.
- [40] Yiming Gao, Yan-Pei Cao, and Ying Shan. Surfelfnerf: Neural surfel radiance fields for online photorealistic reconstruction of indoor scenes. In *Proceedings of the IEEE/CVF Conference on Computer Vision and Pattern Recognition*, pages 108–118, 2023.
- [41] Kaiming He, Xiangyu Zhang, Shaoqing Ren, and Jian Sun. Deep residual learning for image recognition. In *Proceedings of the IEEE conference on computer vision and pattern recognition*, pages 770–778, 2016.
- [42] Alexey Dosovitskiy, Lucas Beyer, Alexander Kolesnikov, Dirk Weissenborn, Xiaohua Zhai, Thomas Unterthiner, Mostafa Dehghani, Matthias Minderer, Georg Heigold, Sylvain Gelly, et al. An image is worth 16x16 words: Transformers for image recognition at scale. *arxiv 2020. arXiv preprint arXiv:2010.11929*, 2010.
- [43] Ze Liu, Yutong Lin, Yue Cao, Han Hu, Yixuan Wei, Zheng Zhang, Stephen Lin, and Baining Guo. Swin transformer: Hierarchical vision transformer using shifted windows. In *Proceedings of the IEEE/CVF international conference on computer vision*, pages 10012–10022, 2021.
- [44] Mingxing Tan and Quoc Le. Efficientnet: Rethinking model scaling for convolutional neural networks. In *International conference on machine learning*, pages 6105–6114. PMLR, 2019.
- [45] Robert T Collins. A space-sweep approach to true multi-image matching. In *Proceedings CVPR IEEE computer society conference on computer vision and pattern recognition*, pages 358–363. Ieee, 1996.
- [46] Sunghoon Im, Hae-Gon Jeon, Stephen Lin, and In So Kweon. Dpsnet: End-to-end deep plane sweep stereo. *arXiv preprint arXiv:1905.00538*, 2019.
- [47] Arda Duzceker, Silvano Galliani, Christoph Vogel, Pablo Speciale, Mihai Dusmanu, and Marc Pollefeys. Deepvideomvs: Multi-view stereo on video with recurrent spatio-temporal fusion. In *Proceedings of the IEEE/CVF Conference on Computer Vision and Pattern Recognition*, pages 15324–15333, 2021.
- [48] Zongwei Zhou, Md Mahfuzur Rahman Siddiquee, Nima Tajbakhsh, and Jianming Liang. Unet++: A nested u-net architecture for medical image segmentation. In *Deep Learning in Medical Image Analysis and Multimodal Learning for Clinical Decision Support: 4th International Workshop, DLMIA 2018, and 8th International Workshop, ML-CDS 2018, Held in Conjunction with MICCAI 2018, Granada, Spain, September 20, 2018, Proceedings 4*, pages 3–11. Springer, 2018.
- [49] Richard Zhang, Phillip Isola, Alexei A Efros, Eli Shechtman, and Oliver Wang. The unreasonable effectiveness of deep features as a perceptual metric. In *Proceedings of the IEEE conference on computer vision and pattern recognition*, pages 586–595, 2018.
- [50] Xiaoshuai Zhang, Sai Bi, Kalyan Sunkavalli, Hao Su, and Zexiang Xu. Nerfusion: Fusing radiance fields for large-scale scene reconstruction. In *Proceedings of the IEEE/CVF Conference on Computer Vision and Pattern Recognition*, pages 5449–5458, 2022.
- [51] Shuaifeng Zhi, Tristan Laidlow, Stefan Leutenegger, and Andrew J. Davison. In-place scene labelling and understanding with implicit scene representation. 2021.
- [52] Diederik P Kingma and Jimmy Ba. Adam: A method for stochastic optimization. *arXiv preprint arXiv:1412.6980*, 2014.

A Appendix / supplemental material

A.1 Experimental Environment

We conduct all the experiments on single NVIDIA RTX A6000 GPU. The experimental environment is PyTorch 2.1.2 and CUDA 12.2.

A.2 Additional Implementation Details

We set the number of virtual depth planes $K = 64$, matching feature dimension $C_m = 16$, and $d_{near} = 0.5, d_{far} = 15.0$ for cost volume formulation, and set $\delta = 0.05$ in Eq.(8) for pixel-wise alignment. During our training and testing, the interval between reference views is set to 20 for ScanNet and 10 for Replica. To train the 3-views version of pixelSplat [1] on a single NVIDIA RTX A6000 GPU, we change their ViT patch size from 8×8 to 16×16 . During inference on the 10 views setting, the epipolar line sampling in pixelSplat and the cross-view attention and cost volume formulation in MVSplat [2] are performed between nearby views similarly as ours to save GPU requirements and form a fair comparison, where for 3-views verion of pixelSplat, MVSplat and FreeSplat we set $N = 2$ to match their training settings, and for the free-view version of FreeSplat we set $N = 4$.

Table 6: Ablation on cost volume framework design.

	3 views				
	PSNR \uparrow	SSIM \uparrow	LPIPS \downarrow	Abs Diff \downarrow	$\delta < 1.25 \uparrow$
MVSplat [2]	24.24	0.769	0.273	0.394	0.625
MVSplat [2] w/o Matched Depth Candidates	24.02	0.754	0.276	0.422	0.574
FreeSplat-spec w/o Matching Net (MN)	26.46	0.801	0.249	0.254	0.840
FreeSplat-spec w/o Multi-Scale Decoder (MSD)	26.07	0.799	0.281	0.263	0.825
FreeSplat-spec w/o (MN+MSD)	24.94	0.767	0.306	0.300	0.776
FreeSplat-spec	27.24	0.820	0.232	0.218	0.882

A.3 Additional Ablation Study

Comparison with MVSplat. Since MVSplat [2] shares commons with our method in high-level design of building cost volume for generalizable 3DGS, we explore the key design differences that leads to our performance improvements. As shown in Figure 5, we notice that MVSplat uses the predicted depth as the ray distance instead of the distance to the image plane, which results in mismatching between the cost volume and point unprojection. As shown in Table 6, we evaluate the effectiveness of our matching net and the multi-scale decoder to compare with MVSplat. We also evaluate the influence of the mismatching problem on MVSplat. We use the image features $F_{s=1}^t$ for cost volume formulation when the matching net is removed. We upsample and concatenate the cost volume with $F_{s=0}^t$ to predict pixel-aligned Gaussian triplets when the multi-scale decoder is removed. The results indicate that removing the matching net (MN) and the multi-scale decoder (MSD) can result in decreased performance on novel view synthesis and depth estimation. Our performance becomes similar as MVSplat when both MN and MSD are removed, which indicates that our cost volume encoding and decoding is more suitable for aggregating more nearby views and can work more effectively on real-world image sequences with complicated camera poses.

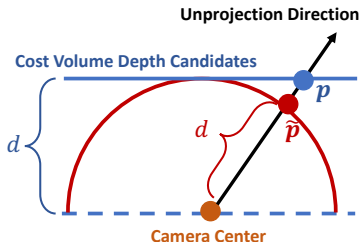


Figure 5: Mismatched depth plane candidates and unprojection in MVSplat [2].

Correlation between view number and performance. To evaluate the influence of changing the number of input views during inference on our method, we conduct an ablation study as shown in Table 7. The results indicate that training on one specific number of input views can lead to notiable performance decrease when inference on different number of views. However, our free-view training strategy can mitigate such correlation, such that to fit to arbitrary number of input views. On 10-views

Table 7: Ablation on the correlation between performance and the number of input views.

	PSNR \uparrow	SSIM \uparrow	LPIPS \downarrow	Abs Diff \downarrow	$\delta < 1.25 \uparrow$
FreeSplat-3views \rightarrow 2views	25.70	0.808	0.240	0.293	0.747
FreeSplat-8views \rightarrow 2views	26.35	0.803	0.242	0.228	0.842
FreeSplat-2views	27.70	0.826	0.222	0.239	0.833
FreeSplat- f_v	27.18	0.818	0.226	0.220	0.847
FreeSplat-8views \rightarrow 10views	24.92	0.788	0.276	0.153	0.926
FreeSplat- f_v \rightarrow 10views	24.91	0.792	0.278	0.159	0.917

setting, our FreeSplat- f_v can still perform similarly as FreeSplat-8views, indicating that using varying number of input views does not harm the long sequence reconstruction results.

A.4 Additional Qualitative Results

2 and 3-View Interpolation Results. The qualitative results are shown in Figure 6, where FreeSplat more precisely localizes 3D Gaussians and captures more fine-grained details comparing to previous methods. FreeSplat can also localize 3D Gaussians more accurately and renders precise depth maps, supporting high-quality rendering from broader view range (*cf.* FreeSplat-*spec* results in Figure 3).

Results on Replica. We show the qualitative results on Replica in Figure 8, where our superiority over MVSPlat and pixelSplat remains. The results indicate the generalization ability of FreeSplat across indoor datasets for the view interpolation task.

Results of Whole Scene Reconstruction. We also show qualitative results of our whole scene reconstruction in Figure 7. Despite the long input sequence (~ 40 images) covering the whole scene, FreeSplat can still perform efficient feed-forward in $\sim 1s$ on single NVIDIA RTX A6000, and can render high-quality images and accurate depth maps from novel views. On the other hand, it’s still difficult to accurately predict depth of textureless (*e.g.* wall) and specular (*e.g.* light reflection on the floor) regions. However, we hope our work provides an initial step towards accurate geometry reconstruction without ground truth depth priors.

A.5 Limitations

Although our approach excels in novel view rendering depth estimation and support arbitrary number of input views, the GPU requirement becomes expensive ($> 40GB$) when inputting extremely long image sequence (> 50). On the other hand, due to our unsupervised scheme of depth estimation, there is still a gap between our 3D reconstruction accuracy and the state-of-the-art methods with 3D supervision [33, 32] or RGB-D inputs [36, 35]. Our main focus is to explore the feed-forward indoor scene photorealistic reconstruction purely based on 2D supervision.

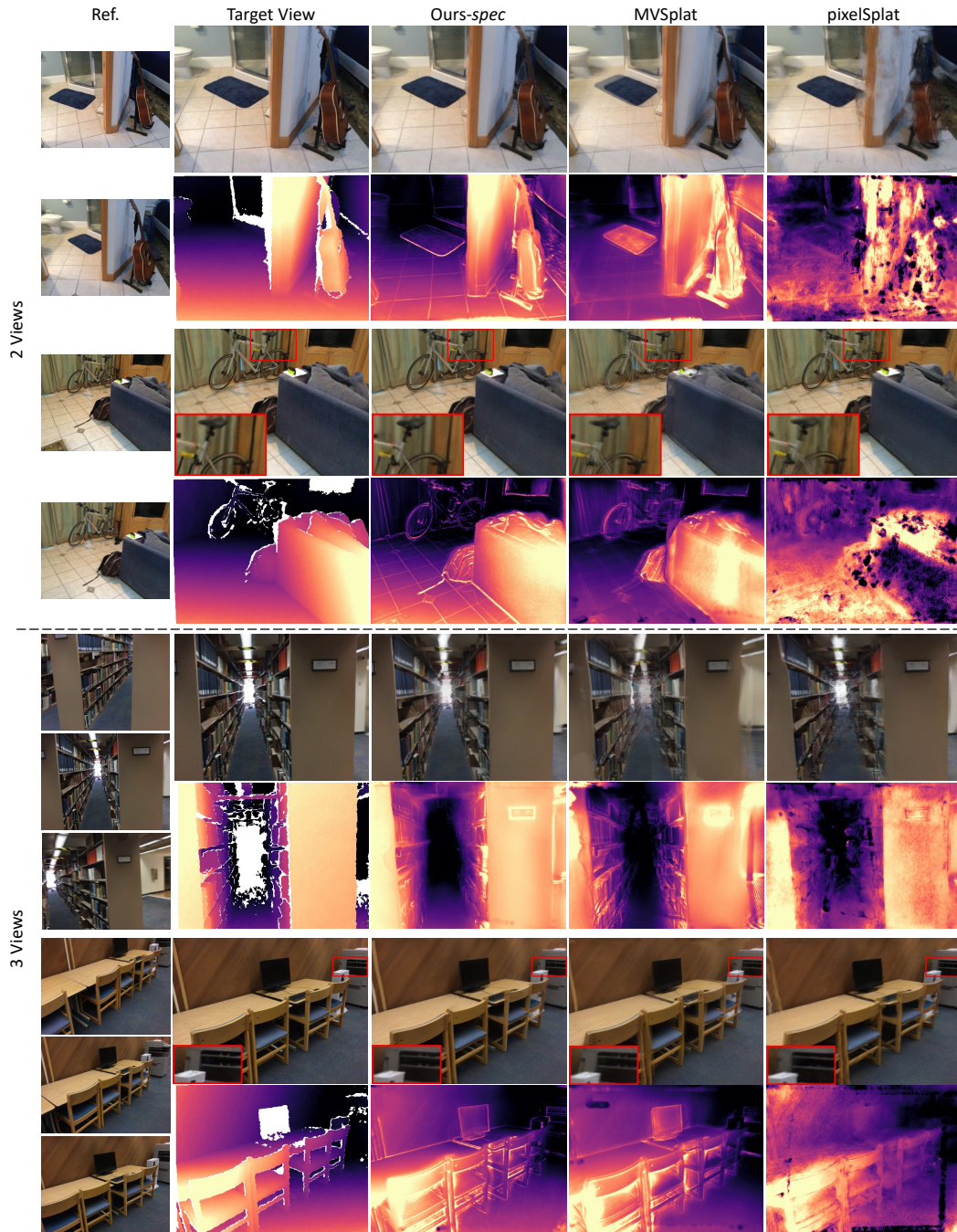


Figure 6: **Qualitative Results given 2 and 3 reference views.** We show the rendered color images (first row) and depth maps (second row) for each batch of reference views.

